J Solid State Electrochem (2012) 16:2349–2356
DOI 10.1007/s10008-012-1668-9

ORIGINAL PAPER

Application of the voltammetry of microparticles for dating archaeological lead using polarization curves and electrochemical impedance spectroscopy

Antonio Doménech-Carbó · María Teresa Doménech-Carbó · María Amparo Peiró-Ronda · Isabel Martínez-Lázaro · Joaquín Barrio-Martín

Received: 15 December 2011 / Revised: 12 January 2012 / Accepted: 14 January 2012 / Published online: 25 February 2012

Abstract The application of the voltammetry of microparticles methodology to date archaeological lead artifacts, based on the time-dependent formation of different layers of lead oxides, whose relative amount can be estimated from polarization curves and electrochemical impedance spectroscopy (EIS), is presented. This approach is complemented by additional data using square wave voltammetry data. Calibration of the method was performed with the help of a series of well-documented, lead pieces from the funds of different Spanish museums, covering since the 7th century BC to nowadays.

A. Doménech-Carbó (✉)
Departament de Química Analítica, Universitat de València,
Dr. Moliner, 50, 46100 Burjassot (València), Spain
e-mail: antonio.domenech@uv.es

M. T. Doménech-Carbó
Institut de Restauració del Patrimoni,
Universitat Politécnica de València,
Camino de Vera 14, 46022 Valencia, Spain

M. A. Peiró-Ronda
Museu de Prehistòria de València,
Corona 36, 46003 Valencia, Spain

I. Martínez-Lázaro
Instituto Valenciano de Conservación y Restauración
de Bienes Culturales de la Generalitat Valenciana,
Penyeta Roja s/n, Castellón, Spain

J. Barrio-Martín
SECYR, Departamento de Prehistoria y Arqueología,
Universidad Autónoma de Madrid,
28049, Madrid, Spain

Keywords Dating · Archaeology · Lead · Voltammetry of microparticles · Electrochemical impedance spectroscopy · Polarization curves

Introduction

Dating is very important in archeometry—but it poses significant problems, in particular in case of metallic samples. With exception of an occasional use of the ^{14}C method performed on the traces of charcoal found in iron objects [1], radiocarbon, uranium-lead radioactive series, and analysis, the main techniques for absolute dating [2, 3], are not used for dating metals [1]. A complementary set of dating procedures can be obtained on the basis of the analysis of the extent of alteration processes on archaeological artifacts, as in case of the obsidian method developed by Friedman and Smith for dating ceramics [4], and the Meissner effect-based method proposed by Reich et al. [1] to estimate the age of archaeological lead.

In a previous report, we presented a method for dating archaeological lead based on the numerical variation of specific features associated to lead corrosion products using the voltammetry of microparticles (VMP) [5]. This method is inspired by that proposed by Scholz, Brainina, Zakharchuk et al. [6], based on electrochemical monitoring of the generation of point defects in ceramic materials by its influence on the electrocatalytic response of such materials used as electrode modifiers. These methods exploit the capabilities of the VMP, a methodology developed by Scholz et al. [7–10] which extends the tradition of solid state electrochemical analysis based on carbon paste electrodes introduced by Adams and

Kuwana et al. [11–13] and significantly developed by Bauer et al. [14], Brainina et al. [15, 16], and Zakharchuk [17, 18] and many others. In the last two decades, VMP has been increasingly used to analyze a wide variety of materials [19–22] and has also been applied in the fields of archaeometry, conservation, and restoration of cultural heritage [23, 24] and offers possibilities for tracing, authentifying, and dating archaeological metals [25, 26].

The aforementioned electrochemical method for dating lead [5] involved the record of the voltammetric response of microparticulate deposits of the corrosion layer of lead pieces on graphite electrodes in contact with aqueous electrolytes. The use of a "one-touch" sampling procedure [27] based on the graphite pencil methodology [28, 29] permitted an essentially non-invasive analysis. Data for both the direct voltammetric response of sample-modified paraffin-impregnated graphite electrodes (PIGEs) and their catalytic effect on the hydrogen and oxygen evolution reactions in aqueous electrolytes were found to be mutually consistent allowing for dating archaeological lead [5].

The use of the proposed methodology is conditioned, however, by the suitability of the simplifying assumptions involved in the procedure [5, 26]: (a) the composition and conditions of aging can be considered as similar for all samples, (b) corrosion proceeded uniformly during the entire corrosion time. Assuming that these conditions hold, calibration from a set of well-documented samples is required.

In this report, we present additional insights into the proposed methodology based on the use of: (a) potentiodynamic polarization curves, and (b) electrochemical impedance spectroscopy. Re-assessment of calibration curves from voltammetric data is also provided upon incorporation of a new set of samples (totaling 25) from different Spanish archaeological sites extending the time interval since the 7th century B.C. to contemporary age. The samples were kindly provided by the Prehistory Museum of Valencia, Archaeological museum of Borriana, museum of Montcada (Spain), Bellas Artes museum of Castelló (Spain) and the SECYR, Departamento de Prehistoria y Arqueología, of the Universidad Autónoma de Madrid.

Experimental

Materials, methods, and instrumentation

Electrochemical experiments were performed using a CH I660C potentiostat. Measurements were performed in 0.10 M $NaClO_4$ (Carlo Erba) and 0.50 M acetic acid/sodium acetate Buffer (Panreac), pH 4.85, in a thermostated three-electrode cell under argon atmosphere using a AgCl (3 M NaCl)/Ag reference electrode and a platinum-wire auxiliary electrode. VMP experiments were performed at sample-modified paraffin-impregnated graphite electrodes (PIGEs) prepared as indicated in literature [7–10]. Polarization curves were obtained at a potential scan rate of 5 mV/s. EIS was carried out using a ±10 mV perturbation signal within a frequency range from 100 kHz to 10 mHz at the open circuit potential (OCP) previously determined for each electrode.

Samples and sampling

Samples include three contemporary pieces (L.1 to L.3) stored in university buildings and 22 genuine archaeological samples (S.3 to S.25) whose location, age, and characteristics are summarized in Table 1. The samples were selected from lead fragments (0.02–0.10 g) separated by the restorers from the original pieces during the process of extraction, cleaning, and/or conservative treatment of the archaeological pieces. Such fragments are systematically conserved and catalogued by the archaeologists and conservators of the museums. The original pieces were all found under burial conditions in calcareous soils in different Spanish locations. Due to corrosion processes often associated to restorative treatments and/or aggressive environments in museum cabinets [30–32], only pristine, not cleaned nor restored rounded pellets or irregular fragments were used for calibration. Figure 1 shows a photographic image of an Iberian plate (4th–2nd BC) discovered in 1996 in La Bastida de les Alcusses, Moixent (Spain), currently in the Prehistory Museum of Valencia. Two fragments accidentally separated from the original piece during its extraction in 1996 constituted samples L.14 and L.15. Sampling was performed by means of the "one touch" methodology already described [27] using 0.2 mm diameter graphite bars. Three replicates of the "one-touch" sampling were performed for each sample upon pressing the graphite bar in different locations of the lead fragment.

Results and discussion

Voltammetric response and corrosion pattern

Figure 2 compares the voltammetric responses for samples L.3 (contemporary patinated lead) and L.19 (from a Phoenician settlement: Tossal Mortorum, Cabanes, Spain) in contact with acetate buffer upon scanning the potential from +0.25 V vs. AgCl/Ag in the negative direction. Here, two main cathodic peaks appear at −0.65 (I) and −0.95 V (II) preceding the rising current for solvent discharge. As previously discussed [5], this voltammetric response can be rationalized on assuming that lead metal is covered by a primary patina, usually constituted by litharge, formed in the atmospheric environment during the usual handling of the piece, and a secondary patina, formed during the last period of utilization and/or the initial stages of various pedological processes (re-crystallization, segregation, desegregation, cementation, monolithizations),

Table 1 Lead samples used in this study

Sample	Description and age	Estimated corrosion time (years)
L.1	Contemporary lead piece	20
L.2	Pipe from university building	50
L.3	Pipe from university building	70
L.4, L.5	Pellets from gunfire, Oropessa castle, 1800-1810. MBAC	200
L.6, L.7, L.8	Irregular piece, Molí Torreblanca, XI-XII AD. MBAC	900
L.9	Inscribed lamina, La Sarsadella, Arabic, X-XI AD. MBAC	1,000
L.10	*Lampadarium* fragment, Punta de l'Illa, visigotic, VI AD. MPV	1,500
L.11	Non-inscribed lamina, Sant Gregori, roman, I AD. MAB	2,000
L.12, L.13	Lead fragments from an Iberian plate. Tossal de Sant Miquel, IV-II BC. MPV.	2,250
L.14, L.15	Lead fragment from an Iberian plate. La Bastida de les Alcusses, Moixent, IV BC. MPV.	2,350
L.16	Lead fragment from an Iberian plate, Tos Pelat, Montcada, VI-IV BC. MMM.	2,500
L.17, L.18	Iberian rolled cylinder, El Pla, Alzira, IV—III BC. MA	2,400
L.19	Irregular fragment Tossal Mortorum Cabanes, phoenician settlement, VII-VI BC. MAB	2,650
L.20, L.21	Irregular fragments, Sant Gregori, I BC. MAB	2,150
L.22, L.23	Irregular fragments, Torrelasal Cabanes, I-BC—I AD. MAB	2,000
L.24, L.25	Irregular fragments, Verdolay, roman, I AD. UAM	1,900

All the pieces selected are non-restored and non-exhibited and belong to the funds of several museums MPV: Museu de Prehistòria de València; MAB: Museu Arqueològic de Borriana; MMM: Museu Municipal de Montcada; MBAC: Museu de Belles Arts de Castelló, Museu de Alzira (MA), and the repository of the SECYR-Departamento de Prehistoria y Arqueología, Universidad Autónoma de Madrid (UAM).

often accompanied by the patina of corrosion which results from processes of diffusion-segregation-deposition [34]. These different layers have different crystallinity, porosity, and degree of hydration similar to lead electrochemically passivated where, depending on the size of the pores, "thermodynamic" and "kinetic" passivation mechanisms can occur [35–39]. In the first mechanism, relatively small pores are formed so that the patina acts as a semi-permeable membrane that allows diffusion of water and H^+, OH^-, and Pb^{2+} ions. The electrochemical process I can be attributed to the reduction of the primary, non-porous PbO patina, whereas the electrochemical process II can be assigned to the reduction of the porous layer resulting from kinetic passivation. In this second case, all

Fig. 1 Photographic image of an Iberian plate (4th–2nd BC) discovered in 1996 in La Bastida de les Alcusses, Moixent (Spain), currently in the Prehistory Museum of Valencia. Sample L.14 was taken from fragments accidentally separated from the original piece during its extraction in 1996

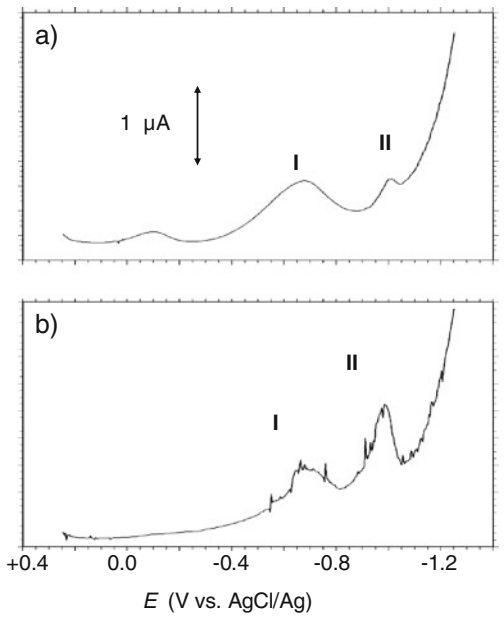

Fig. 2 SWVs for PIGEs modified by means of "one-touch"' methodology for: (a) contemporary lead (L.3); (b) sample L.19 providing from a Phoenician settlement (Tossal Mortorum, Cabanes, Spain) dated 7th–6th BC immersed into 0.50 M HAc/NaAc, pH 4.85. Potential scan initiated at +0.25 V in the negative direction. Potential step increment 4 mV; square wave amplitude 25 mV; frequency 5 Hz

ions can move freely through the pores so that when the reaction can proceed at the pore orifice near the electrolyte, thus resulting in a peak potential clearly separated from that of process I. In agreement with VMP studies of lead oxides due to Zakharchuk et al. [40] and Scholz et al. [41, 42], the electrochemical reduction of PbO to Pb can be described in terms of a topotactic solid state transformation of lead oxide to lead metal without a morphological disintegration, possibly superimposed to reduction involving intermediate Pb^{2+} ions in solution phase further reduced to lead metal [40–43].

If the potential scan is initiated at +1.25 or more positive potentials, additional voltammetric signals attributable to the reduction of PbO_2 (or possibly PbO_n ($1<n<2$)) species appear. As shown in Fig. 3, such signals are clearly larger for archaeological lead than for contemporary lead. This feature suggests that PbO_n materials are formed during prolonged corrosion, so that such voltammetric features can be used for dating archaeological lead artifacts [5]. The formation of α- and β-PbO_2 and substoichiometric lead oxides can explain the multiple peak profile observed for PbO_2-modified electrodes immersed into acetate buffer [40, 44–46]. As already described, voltammograms obtained upon scanning the potential in the positive direction from potentials ca. −1.0 V archaeological samples show stripping oxidation peaks for antimony, arsenic, bismuth and copper accompanying the prominent signal for the stripping of lead, thus providing an additional criterion for authentication [25, 26].

Voltammetric dating

As previously reported [5], under the previously noted simplifying assumptions, one can assume that the peak height (or the peak area) of process II (A_{II}) is representative, under fixed electrochemical conditions (electrolyte, potential scan rate, etc.), of the amount of corrosion layer plus base patina formed during the corrosion process while the area of the peak I (A_I) would be representative of the amount of base patina. Assuming that the corrosion process is based on the local existence of an electrochemical cell which comprises a junction of metallic oxide to a metal surface and the oxygen/water couple, the corrosion rate follows a potential law [1, 47] so that the above peak areas should satisfy the relationship:

$$\frac{A_{II}}{A_I} = G_1 + [G_2(1+\alpha)t]^{1/(1+\alpha)} \quad (1)$$

Here, G_1 and G_2 are constants depending on the mass of primary patina by surface unit. This can be taken as essentially identical for all samples so that Eq. (1) predicts a linear relationship between the (A_{II}/A_I) ratio and $t^{1/(1+\alpha)}$ for the appropriate value of the coefficient α. Previous data using peak currents provided a satisfactory fit between theory and experimental data taking $\alpha=0.070$, a value that is identical to that obtained by Reich et al. [1] using measurements on the Meissner fraction in the superconducting state of lead.

Under our experimental conditions, the best results were obtained for peak areas measured as schematized in Fig. 4. Using such peak areas, the standard deviation of the A_{II}/A_I ratio upon repetitive "one-touch" experiments on the same sample becomes between 5% and 8%. In spite of relatively large data dispersion, the representation of the A_{II}/A_I ratio vs. $t^{0.935}$ (corresponding to $t^{1/(1+\alpha)}$ for $\alpha=0.07$) can satisfactorily be fitted to a straight line, as can be seen in Fig. 5.

Polarization curves

Potentiodynamic polarization curves have been extensively used in corrosion studies. Figure 6 shows typical polarization curves obtained for the studied samples attached to

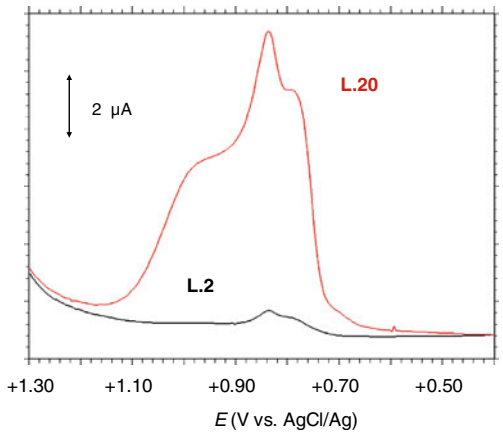

Fig. 3 Detail of SWVs for PIGEs modified by means of "one-touch" methodology for contemporary lead (L.2) and sample L.20 immersed into 0.50 M HAc/NaAc, pH 4.85. Potential scan initiated at +1.45 V in the negative direction. Potential step increment 4 mV; square wave amplitude 25 mV; frequency 5 Hz

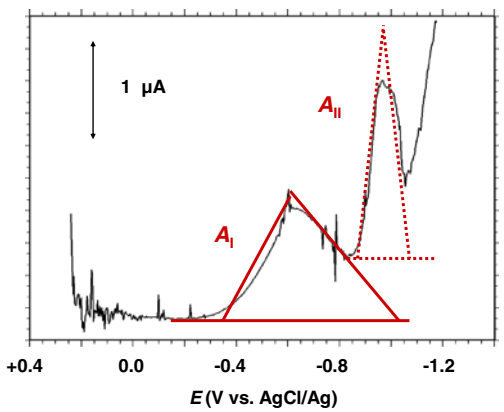

Fig. 4 Criterion used to measure peak areas for the electrochemical processes I and II in SWVs of sample-modified PIGEs immersed into acetate buffer. The voltammogram corresponds to sample L.20; conditions such as in Fig. 2

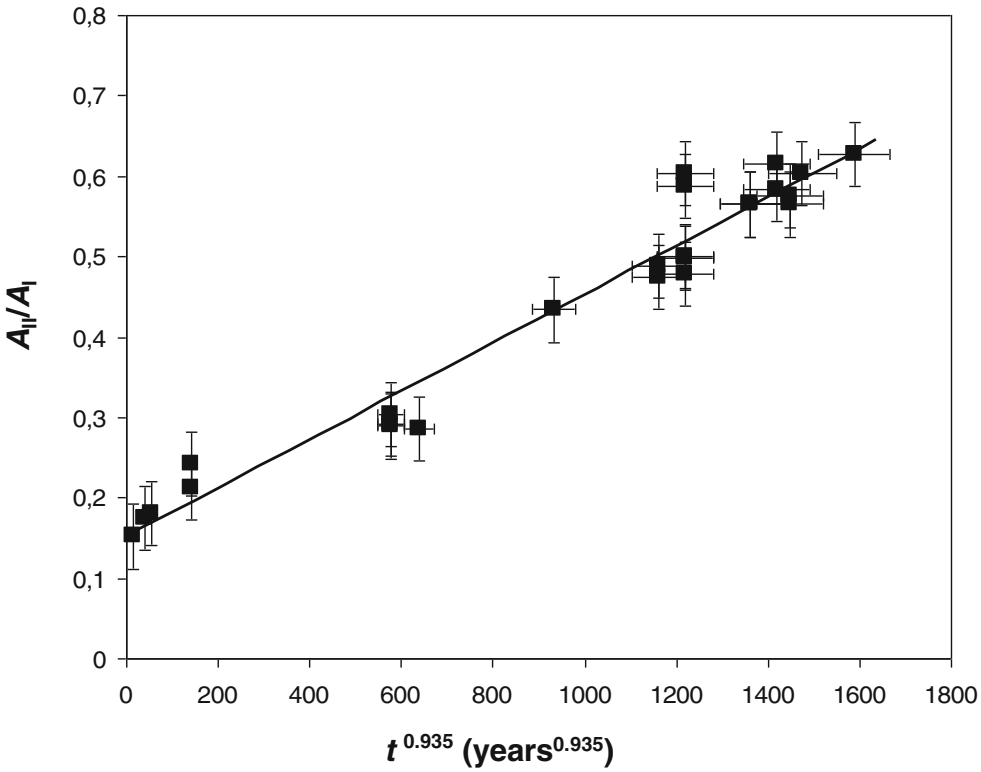

Fig. 5 Plots of i_{II}/i_I vs. $t^{1/(1+\alpha)}$ for α=0.07 for samples in this study. From SWVs at PIGEs modified with the samples via "one-touch" methodology. Electrolyte 0.50 M HAc/NaAc, pH 4.85. Conditions such as in Fig. 2

PIGEs via "one-touch" sampling immersed into 0.10 M $NaClO_4$ when the potential is scanned from −0.65 V in the positive direction. One sharp corrosion peak, often exhibiting peak splitting is recorded at potentials between −0.40 and −0.65 V. This is preceded by an inclined log*i* vs. *E* branch and followed by an almost horizontal branch, suggesting that a passivation behavior occurs at potentials up to −0.40 V. The profile of this region varies significantly in replicate experiments for the same sample, thus suggesting that the amount of sample and its more or less efficient adherence to the graphite electrode affect significantly the polarization response, a result that is consistent with the microparticulate nature of the studied deposit and the peculiar characteristics of the "one-touch" sampling. In contrast, the potential region preceding the peak varies slightly in replicate experiments for each sample, the dispersion of the apparent inverse Tafel slope (*ATSL*) of the corresponding E_p vs. log*i* representation remaining ca. 5–10% for experiments in 0.10 M $NaClO_4$. Interestingly, the *ATSL* of contemporary lead was clearly larger than those determined for archaeological samples. Figure 7 shows the calibration curve

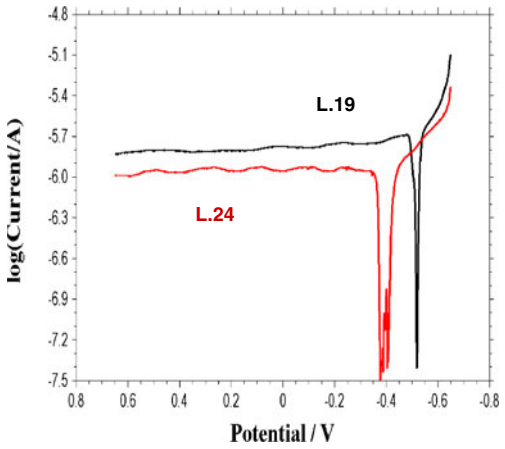

Fig. 6 Potentiodynamic polarization curves for samples L.19 and L.24 attached to PIGEs in contact with 0.10 M $NaClO_4$. Potential scan initiated at −0.65 V in the positive direction; potential scan rate 5 mV/s

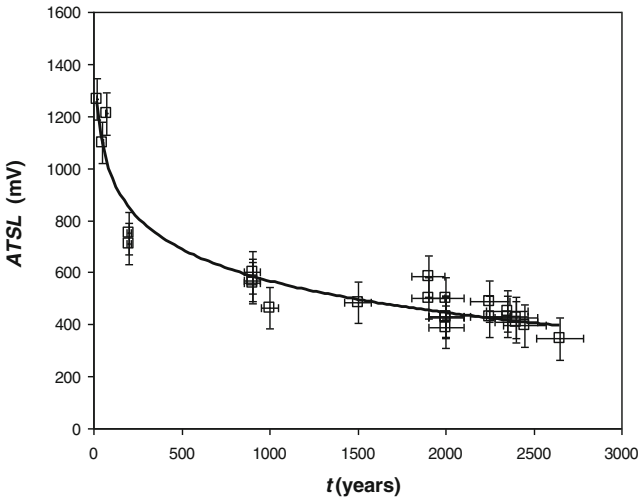

Fig. 7 Calibration curve to date archaeological lead using the apparent inverse Tafel slope determined in polarization curves for sample-modified PIGEs immersed into 0.10 M $NaClO_4$ in conditions such as in Fig. 6

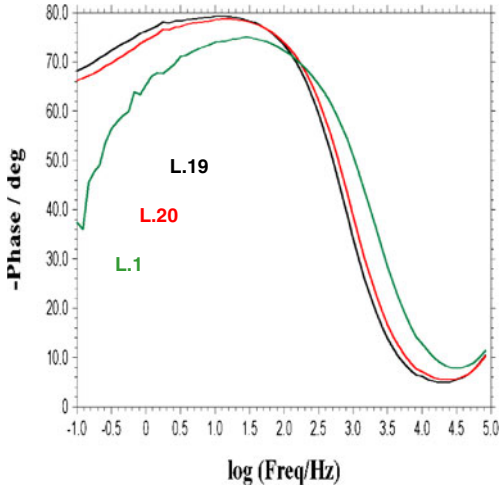

Fig. 8 Bode phase angle vs. log (frequency) plots for contemporary lead (L.1) and samples L19 and L.20 immersed into 0.50 M HAc/NaAc at pH 4.85

consisting of the representation of *ATSL* vs. corrosion time. Polarization curves for sample-modified PIGEs in contact with acetate buffer were similar, but the dispersion of apparent Tafel slopes was clearly larger than 10%.

Electrochemical impedance spectroscopy

Impedance spectra measured at OCP yield similar features for tested samples in contact with both $NaClO_4$ and HAc/NaAc electrolytes. Bode plots of log (total impedance) vs. log (frequency) (log*Z* vs. log*f*) consist of typical s-shaped curves with log*Z* monotonically decreasing on increasing log*f*. Bode plots of phase angle vs. log (frequency) (φ vs. log*f*), shown in Fig. 8 are close to those expected for metals covered by a coating where diffusive effects play a significant role, as recently described by Cano et al. [33]. Consistently, Nyquist plots (see Fig. 9) consist of a capacity depressed semicircle with a distinctive 45° tail in the low-frequency region, attributable to

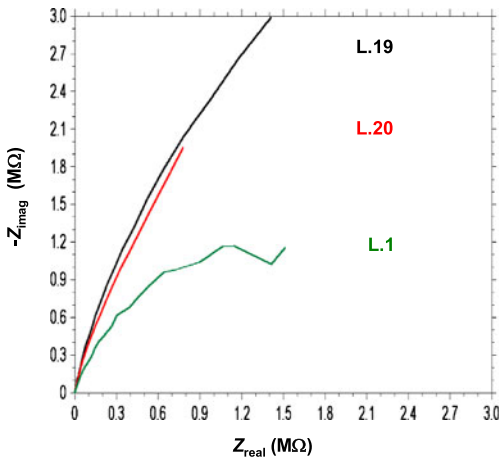

Fig. 9 Nyquist plots for contemporary lead (L.1) and samples L19 and L.20 in contact with 0.10 M $NaClO_4$

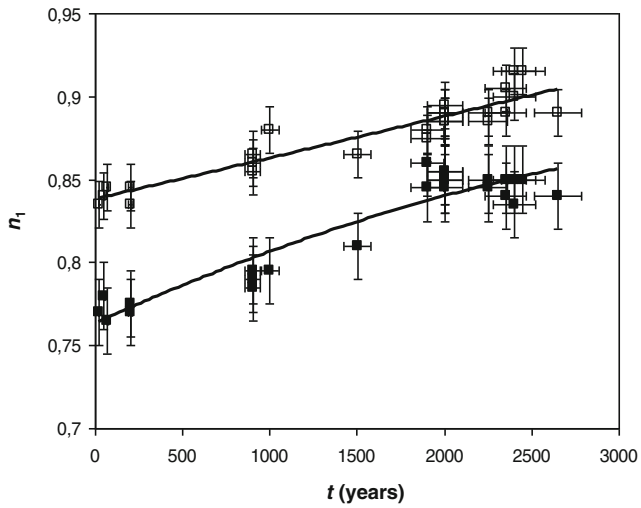

Fig. 10 Calibration plots shown the variation of the apparent CPE1 exponent, n_1, with the corrosion time for samples in this study. Data from EIS experiments at the OCP for sample-modified PIGEs immersed into 0.50 M HAc/NaAc and 0.10 M $NaClO_4$ electrolytes

the diffusion of species through the pores of the corrosion products [48–51] and/or protective coatings [52–55]. The semicircle depression (i.e., the rotation of the semicircle center by an angle below the real axis) can be attributed, at least partially, to surface roughness, but also to cell geometry giving rise to time constant dispersion [55–57].

This EIS response can in principle be modeled by an equivalent circuit constituted by a solution resistance, R_s, in series to a parallel combination of constant phase element (CPE1), and a series combination of a second constant phase element (CPE2) plus a charge transfer resistance, R_{ct} [33]. This last element can be associated to the points where the solution reaches the metal surface and corrosion occurs, whereas the CPE element could be regarded as representative of the diffusion of species through the corrosion layers

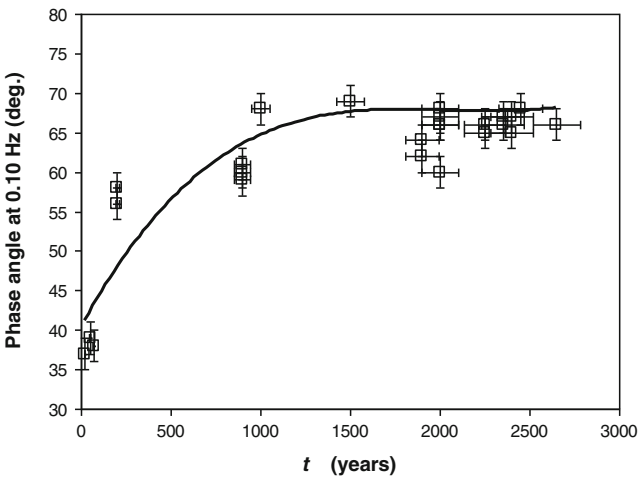

Fig. 11 Variation of the phase angle at 0.10 Hz with the corrosion time for samples in this study. From EIS experiments at the OCP for sample-modified PIGEs immersed into 0.10 M $NaClO_4$

(which could be represented as a Warburg element in the case of uncomplicated diffusion [58]). The impedance of the CPE elements is given by $Z_{CPE}=1/H(j\omega)^n$, where H is a constant and ω the angular frequency.

The CPE1 replaces the usual double layer capacitance, C_{dl}, and accounts for non-ideal capacitive behavior of the interfacial charge transfer mechanism associated with the nonuniform distribution of current as a result of roughness and surface defects which results from surface roughness, impurities, dislocations, or grain boundaries [59–63]. The CPE2 is representative of the non-ideal diffusive behavior associated to the permeation of the corrosion layers and could be also modeled by means of a Warburg impedance. More elaborated modeling of corroded metal surfaces involve inserting additional elements in order to represent the bi- or multilayer nature of the corrosion coatings [64, 65].

On comparing the EIS response for the different samples, it was found that the main differences were placed in the region of intermediate frequencies, corresponding to light variations in the CPE exponent n_1, and particularly in the low frequency region. As can be seen in Fig. 8, for contemporary lead the Bode plot becomes close to that expected by metals covered by a coating where no important diffusive contribution occurs [33], thus becoming clearly separated from the corresponding plots recorded for archaeological samples. Consistently, the Nyquist plot for contemporary lead (see Fig. 9) shows an almost complete semicircle clearly diverging from the previously described features recorded for archaeological lead samples.

As far as the corrosion layers can influence the double layer capacitance (represented by the CPE1) and the diffusive regime at low frequencies (represented by CPE2), the variation of the exponent of the constant phase element (n_1) determined using the aforementioned equivalent circuit, with the corrosion time was tested for calibration purposes. On first examination, an apparent value of the CPE1 exponent n_1 can be estimated from experimental data as the slope of the log$Z$ vs. log$f$ plots in the intermediate region of frequencies. The relevant point to emphasize is that n_1 should increase on increasing the importance of the roughness of the corrosion layers covering the metal surface [59–63], so that it appears reasonable to expect that, assuming uniform conditions of corrosion, apparent n_1 values increase with the corrosion time. As can be seen in Fig. 10, where EIS data for sample-modified PIGEs immersed into 0.50 M HAc/NaAc and 0.10 M $NaClO_4$ electrolytes are shown, experimental data for the studied samples agree with the foregoing set of considerations, the apparent n_1 values increasing monotonically with corrosion time. Similarly, the phase angle at 0.10 Hz (see Fig. 8), a quantity easily obtained from experimental data without need of modeling, varied significantly from contemporary lead to archaeological samples. Figure 11 shows the corresponding representation. In this case, however, the phase angle varies remarkably from contemporary lead to archaeological one, but the variations within the archaeological samples are small. Although this parameter would be not sensitive to changes in the corrosion time, it is of value to provide a clear distinction between contemporary and archaeological lead.

Conclusions

Application of "one-touch" sampling to transfer nanosamples from archaeological lead objects onto the surface of graphite electrodes permits to obtain specific signatures for PbO_n and PbO formed during the corrosion process under burial conditions able to be used for dating purposes. Dating is based on the time-dependent formation of different layers of such lead oxides, whose relative amount can be estimated from electrochemical data. The ratio between peak current areas for primary and secondary corrosion layers in such VMP experiments can satisfactorily be fitted to a potential rate law using the voltammetric peaks recorded for lead samples in contact with aqueous acetate buffer. The apparent Tafel slope obtained in polarization curves for sample-modified electrodes immersed into 0.10 M $NaClO_4$ also provides a variation with the corrosion time suitable for dating purposes.

The EIS behavior of sample-modified graphite electrodes presents significant differences in the low frequency region which can be mainly attributed to different permeability to diffusion of the corrosion layers. The exponent of the constant phase element introduced in modeling the equivalent circuit also varies systematically with the corrosion time.

The reported data act in support of the idea that electrochemical measurements, in spite of the limitations associated to the necessary simplifying assumptions, can provide a reasonable approach for dating archaeological lead artifacts.

Acknowledgements Financial support is gratefully acknowledged from the MEC Projects CTQ2011-28079-CO3-01 and 02 which are also supported with ERDF funds. Research was conducted within the "Grupo de análisis científico de bienes culturales y patrimoniales y estudios de ciencia de la conservación" Microcluster of the University of Valencia Excellence Campus. The collaboration of the Museu de Prehistòria de València, Museu Arqueològic de Borriana; Museu Municipal de Montcada; Museu de Belles Arts de Castelló, Museu de Alzira and the SECYR-Departamento de Prehistoria y Arqueología, Universidad Autónoma de Madrid (UAM) is gratefully acknowledged.

References

1. Reich S, Leitus G, Shalev S (2003) New J Phys 5:99.1–99.9
2. Aitken MJ (1990) Science-Based Dating in Archaeology. Longman, New York; chapter 8
3. Renfrew C, Bahn P (1991) Archaeology: Theory, Methods and Practice. Thames & Hudson, London; chapter 4
4. Friedman I, Smith RL (1960) Amer Antiq 25:476–493

5. Doménech A, Doménech MT, Peiró MA (2011) Anal Chem 83:5639–5644
6. Scholz F, Schröder U, Meyer S, Brainina KhZ, Zakharchuk NF, Sobolev NV, Kozmenko OA (1995) J Electroanal Chem 385:139–142
7. Scholz F, Nitschke L, Henrion G (1989) Naturwiss 76:71–72
8. Scholz F, Nitschke L, Henrion G, Damaschun F (1989) Naturwiss 76:167–168
9. Scholz F, Nitschke L, Henrion G (1989) Fresenius Z Anal Chem 334:56–58
10. Scholz F, Nitschke L, Henrion G, Damaschun F (1989) Fresenius Z Anal Chem 335:189–194
11. Adams RN (1958) Anal Chem 30:1576
12. Kuwana T, French WG (1964) Anal Chem 36:241–242
13. Schultz FA, Kuwana T (1965) J Electroanal Chem 10:95–103
14. Bauer D, Gaillochet MP (1974) Electrochim Acta 19:597–606
15. Brainina KhZ, Lesunova RP (1974) Zh Anal Khim 29:1302–1308
16. Brainina KhZ, Vidrevich MB (1981) J Electroanal Chem 121:1–28
17. Belyi VI, Smirnova TP, Zakharchuk NF (1989) Appl Surf Sci 39:161–167
18. Belyi VI, Smirnova TP, Zakharchuk NF (1989) Thin Solid Films 113:57–164
19. Scholz F, Meyer B (1998) Electroanal Chem A Series Adv 20:1–86
20. Grygar T, Marken F, Schröder U, Scholz F (2002) Collect Czech Chem Commun 67:163–208
21. Scholz F, Schröder U, Gulabowski R (2005) Electrochemistry of immobilized particles and droplets. Springer, Berlin
22. Hermes M, Scholz F (2009) in Solid State Electrochemistry I, Kharton VV, Ed. Wiley-VCH, Weinheim; chapter 6
23. Doménech A, Doménech MT, Costa V (2009) In: Scholz F (ed) Electrochemical methods in archaeometry, conservation and restoration, Monographs in Electrochemistry series. Springer, Berlin
24. Electrochemistry for Conservation Science (2010) Doménech A Ed. J Solid State Electrochem 14, No. 3
25. Doménech A, Doménech MT, Peiró MA, Osete L (2011) Archaeometry 53:1193–1211
26. Doménech A (2011) Anal Methods 3:2181–2188
27. Doménech A, Doménech MT, Peiró MA (2011) Electroanal 23:1391–1400
28. Blum D, Leyffer W, Holze R (1996) Electroanalysis 8:296–297
29. Costa V, Dubus M (2007) Impact of the environmental conditions on the conservation of metal artifacts: an evaluation using electrochemical techniques, in Museum Microclimates, Padfield T, Ed. The National Museum of Denmark, pp 63–65
30. Cano E, Bastidas JM (2006) Conservación preventiva de metales en interiores: control de la contaminación por ácidos orgánicos, in Tecnología y conservación del Patrimonio Arqueológico/I: Innovación tecnológica en conservación y restauración del Patrimonio. CENIM-UAM, Madrid
31. Tétreault J, Cano E, Van Bommel M, Scott D, Dennis M (2003) Stud Conservat 48:237–250
32. Degrigny C (2010) J Solid State Electrochem 14:353–361
33. Cano E, Lafuente D, Bastidas DM (2010) J Solid State Electrochem 14:381–391
34. Sandu I, Marutoiu C, Sandu IG, Alexandru A, Sandu AV (2006) Acta Universitatis Cibinensis Sect F Chemia 9:39–53
35. Pavlov D (1968) Electrochim Acta 13:2051–2061
36. Pavlov D, Popoda R (1970) Electrochim Acta 15:1483–1491
37. Pavlov D, Monakhov B (1987) J Electroanal Chem 218:135–153
38. Pavlov D, Monakhov B, Salmi K, Sundholm G (1991) Electrochim Acta 36:953–963
39. Cai W-B, Wan Y-Q, Liu H-T, Zhou W-F (1995) J Electroanal Chem 387:95–100
40. Zakharchuk N, Meyer S, Lange B, Scholz F (2000) Croat Chem Acta 73:667–704
41. Meyer B, Ziemer B, Scholz F (1995) J Electroanal Chem 392:79–83
42. Hasse U, Scholz F (2001) Electrochem Commun 3:429–434
43. Doménech A, Doménech MT, Mas X (2007) Talanta 71:1569–1579
44. Pavlov D (1981) J Electroanal Chem 118:167–185
45. Bartlett PN, Dunford T, Ghanem MA (2002) J Mater Chem 12:3130–3135
46. Pavlov D, Monakhov B (1989) J Electrochem Soc 136:27–33
47. Chilton JP (1968) Principles of metallic corrosion. The Royal Institute of Chemistry, London
48. Walter GW (1981) J Electroanal Chem 118:259–273
49. Chiavari C, Colledan A, Frignani A, Brunoro G (2006) Mater Chem Phys 95:252–259
50. Chiavari C, Rahmouni K, Takenouti H, Joiret S, Vermaut P (2007) Electrochim Acta 52:7760–7769
51. Skale S, Dolecek V, Slemnik M (2007) Corros Sci 49:1045–1055
52. Murray JN (1997) Progr Org Coat 31:375–391
53. Bastidas JM, Polo JL, Torres CL, Cano E (2001) Corros Sci 43:269–281
54. Polo JL, Cano E, Bastidas JM (2002) J Electroanal Chem 537:183–187
55. Polo JL, Cano E, Kong DY, Bastidas JM (2002) Corrosion 58:670–674
56. Silverman DC (1989) Corrosion 45:824–830
57. Bastidas JM, Polo JL, Cano E, Torres CL, Mora N (2000) Mater Corros 51:712–718
58. Growcock FB, Jasinski RJ (1989) J Electrochem Soc 136:2310–2314
59. Martini EMA, Muller IL (2000) Corros Sci 42:443–454
60. Alves VA, Brett CMA (2002) Electrochim Acta 47:2081–2091
61. Li WS, Cai SQ, Luo JL (2004) J Electrochem Soc 151:B220–B226
62. Liu W, Zhang H, Qu Z, Zhang Y, Li J (2010) J Solid State Electrochem 14:965–973
63. Toledo-Martos LA, Pech-Canul MA (2011) J Solid State Electrochem 15:1927–1934
64. Evesque M, Keddam M, Takenouti H (2004) Electrochim Acta 49:2937–2943
65. Lee JJ, Pyun SI (2007) J Solid State Electrochem 11:829–839